Mitochondrial dysfunction and oxidative stress contribute to cognitive and motor impairment in FOXP1 syndrome

Jing Wang[a,1], Henning Fröhlich[a,1], Felipe Bodaleo Torres[b], Rangel Leal Silva[b], Gernot Poschet[c], Amit Agarwal[b,d], and Gudrun A. Rappold[a,d,2]

[a]Department of Human Molecular Genetics, Institute of Human Genetics, Heidelberg University Hospital, D-69120 Heidelberg, Germany; [b]Chica and Heinz Schaller Research Group, Institute for Anatomy and Cell Biology, D-69120 Heidelberg, Germany; [c]Metabolomics Core Technology Platform, Centre for Organismal Studies, University of Heidelberg, D-69120 Heidelberg, Germany; and [d]Interdisciplinary Center for Neurosciences, University of Heidelberg, D-69120 Heidelberg, Germany

Edited by Hugo Bellen, Departments of Molecular and Human Genetics, and Neuroscience, Baylor College of Medicine, Houston, TX; received July 14, 2021; accepted December 28, 2021

FOXP1 syndrome caused by haploinsufficiency of the forkhead box protein P1 (FOXP1) gene is a neurodevelopmental disorder that manifests motor dysfunction, intellectual disability, autism, and language impairment. In this study, we used a *Foxp1*$^{+/-}$ mouse model to address whether cognitive and motor deficits in FOXP1 syndrome are associated with mitochondrial dysfunction and oxidative stress. Here, we show that genes with a role in mitochondrial biogenesis and dynamics (e.g., *Foxo1*, *Pgc-1α*, *Tfam*, *Opa1*, and *Drp1*) were dysregulated in the striatum of *Foxp1*$^{+/-}$ mice at different postnatal stages. Furthermore, these animals exhibit a reduced mitochondrial membrane potential and complex I activity, as well as decreased expression of the antioxidants superoxide dismutase 2 (Sod2) and glutathione (GSH), resulting in increased oxidative stress and lipid peroxidation. These features can explain the reduced neurite branching, learning and memory, endurance, and motor coordination that we observed in these animals. Taken together, we provide strong evidence of mitochondrial dysfunction in *Foxp1*$^{+/-}$ mice, suggesting that insufficient energy supply and excessive oxidative stress underlie the cognitive and motor impairment in FOXP1 deficiency.

FOXP1 syndrome | ASD | cognitive and motor impairment | mitochondrial defect | ROS

Autism spectrum disorder (ASD) is a neurodevelopmental disorder characterized by impaired social communication, restricted or stereotypical interests, and repetitive behaviors. Molecular genetic studies on ASD individuals and their families have identified several hundred ASD risk genes, including the forkhead box protein P1 (*FOXP1*) gene. In humans, haploinsufficiency of *FOXP1* leads to FOXP1 syndrome (Online Mendelian Inheritance in Man [OMIM] 605515), a neurodevelopmental disorder characterized by delayed motor and language development, intellectual disability, autistic traits, and dysmorphic features (1, 2). Since the first report in 2010 (1), more than hundred cases with de novo mutations have been described in the literature, and *FOXP1* is now among the highest ranked ASD genes according to the Simons Foundation Autism Research Initiative (SFARI) Gene database (3).

FOXP1 is a member of the Forkhead Box P (FOXP) subfamily of transcription factors, which also includes FOXP2, FOXP3, and FOXP4. Both FOXP1 and FOXP2 are highly conserved in vertebrates and form homo- and heterodimers (4, 5), and while *FOXP2* mutations have been linked with a distinct speech and language disorder (6), *FOXP1* mutations affect much more global neural functions. They may also form oligomers with FOXP4 (5), suggesting that these three related transcription factors regulate cognitive behavior and motor development via common pathways (7).

The complete loss of *Foxp1* in mice is lethal at embryonic day 14.5 (E14.5) (8), but the phenotype of heterozygous *Foxp1*$^{+/-}$ mice resembles that of individuals with FOXP1 syndrome. *Foxp1*$^{+/-}$ animals exhibit behavioral and muscle deficits such as reduced neonatal ultrasonic vocalization and grip strength (9), that are first indications for social deficits and hypotonia in animals. Furthermore, *Foxp1*$^{+/-}$ mice display esophageal achalasia and impaired peristalsis in the colon (10), reflecting the gastrointestinal disturbances seen in many individuals with FOXP1 syndrome (2, 11).

In the brain, Foxp1 is mainly expressed in the cortex, hippocampus, and striatum (7, 12). In the cortex, Foxp1 is mainly expressed in the intratelecephalic projection neurons in layers 3 to 5, regulating neonatal vocalizations (13). In the hippocampus, Foxp1 expression is seen in the CA1 subfield and subiculum region, required for spatial learning and synaptic plasticity (14). In the striatum, Foxp1 has been shown its most abundant expression and to regulate the cellular composition and connectivity in a cell type–specific manner (15). Thus, Foxp1 has an essential role in regulating neurogenesis and synapse organization. However, the role of Foxp1 and its transcriptional regulators have not been studied on metabolic disturbances and

Significance

***FOXP1* haploinsufficiency underlies cognitive and motor impairments in individuals with FOXP1 syndrome. Here, we show that mice lacking one *Foxp1* copy exhibit similar behavioral deficits, which may be caused by striatal dysfunction. Indeed, *Foxp1*$^{+/-}$ striatal medium spiny neurons display reduced neurite branching, and we show altered mitochondrial biogenesis and dynamics; increased mitophagy; reduced mitochondrial membrane potential, structure, and motility; and elevated oxygen species in the striatum of these animals. As *FOXP1* is highly conserved, our data strongly suggest that mitochondrial dysfunction and excessive oxidative stress contribute to the motor and cognitive impairments seen in individuals with FOXP1 syndrome. Thus, mitochondrial homeostasis is critical for normal development and can explain deficits in neurodevelopmental disorders.**

Author contributions: J.W., H.F., A.A., and G.A.R. designed research; J.W., H.F., F.B.T., R.L.S., and G.P. performed research; J.W., H.F., F.B.T., and R.L.S. analyzed data; and J.W., H.F., A.A., and G.A.R. wrote the paper.

The authors declare no competing interest.

This article is a PNAS Direct Submission.

[1]J.W. and H.F. contributed equally to this work.

[2]To whom correspondence may be addressed. Email: gudrun.rappold@med.uni-heidelberg.de.

This article contains supporting information online at http://www.pnas.org/lookup/suppl/doi:10.1073/pnas.2112852119/-/DCSupplemental.

Published February 14, 2022.

mitochondrial malfunction. In fact, mitochondrial function plays an important role in neurogenesis, synaptic plasticity, and neurotransmission (16–18).

Metabolic disturbances and mitochondrial malfunctions are also more common in individuals with ASD than in the general population, indicating that they play a role in the pathogenesis of ASD (19, 20). However, only certain subgroups of the ASD population are affected. To investigate whether mitochondrial impairment might underlie the cognitive and motor features of FOXP1 syndrome, we analyzed mitochondrial structure and motility, and the expression of genes that regulate mitochondrial biogenesis and dynamics in the striatum of *Foxp1*$^{+/-}$ mice. We examined autophagy, production of reactive oxidative species (ROS), metabolic status. and apoptosis in these animals. In addition, we analyzed neuronal morphology, motor function, as well as emotional and spatial learning and memory.

Results

Dysregulated Mitochondrial Biogenesis in the *Foxp1*$^{+/-}$ Striatum. Nervous system-specific and conventional *Foxp1* knockout mice (9, 12) and MRI images of FOXP1 syndrome individuals (2, 21) have revealed that the striatum is particularly affected by FOXP1 deficiency. To evaluate Foxp1 expression at early postnatal development as well as adult stage in the striatum, we compared *Foxp1* mRNA and protein level of *Foxp1*$^{+/-}$ to that of wild-type (WT) littermates at postnatal day (P) 1.5, P12.5, and 8 wk. The rational for the choice P1.5 is that at this time of developmental stage the excitatory inputs to the striatum are minimal, by P12.5 the excitatory inputs to the striatum peak, and by 8 wk striatal circuits are fully mature and the mice have complete motor function (22, 23). Additionally, this maturation is accompanied by a significant decrease in *Foxp1* mRNA and protein (both Foxp1 A and Foxp1 D) by ∼41% and ∼52%, respectively, in *Foxp1*$^{+/-}$ mice compared to WT animals (Fig. 1*A* and *SI Appendix*, Figs. S1*A* and S2*A*). *Foxo1*, a target of Foxp1 in the striatum (10, 12), was also significantly lower on mRNA and protein level at all three time points analyzed (Fig. 1*B* and *SI Appendix*, Figs. S1*A* and S2*B*). Foxp1 and Foxo1 interact in liver tissue (24) but not in the striatum as shown by immunoprecipitation, suggesting that a direct Foxp1-Foxo1 interaction does not contribute to the striatal dysfunction in Foxp1-deficient mice (*SI Appendix*, Fig. S1*B*).

The transcription factor Foxo1 is a "nutrient sensor." Depending upon the cellular stress levels, it shuttles between nucleus and mitochondria and binds to mitochondrial DNA (mtDNA) to regulate mitochondrial biogenesis (25, 26). Reduced Foxo1 levels were detected in the cytoplasmic but not in the nuclear fraction of the *Foxp1*$^{+/-}$ striatum (*SI Appendix*, Fig. S1*C*). Thus altered expression of Foxo1 target genes resulting in impaired mitochondrial biogenesis and function might play a role in the developmental defect of the *Foxp1*$^{+/-}$ animals (27–30). To test this hypothesis, we analyzed mRNA levels of *Pparα*, *Pparγ*, *Pgc-1α*, *Nrf1*, *Nrf2*, and *Tfam* at P1.5, P12.5, and 8 wk. The expression of all genes was significantly altered in the *Foxp1*$^{+/-}$ striatum at one or more of the three stages investigated (*SI Appendix*, Fig. S1*D*). In particular, proliferator-activated receptor gamma coactivator 1-alpha (Pgc-1α) and mitochondrial transcription factor A (Tfam) were down-regulated on protein level at all three stages in *Foxp1*$^{+/-}$ striatal tissue (Fig. 1 *C* and *D* and *SI Appendix*, Fig. S2 *C* and *D*), which was not the case for nuclear respiratory factor 1 (Nrf1) (*SI Appendix*, Fig. S2*E*). Moreover, mitochondrial markers Atp5a and Tom20 also showed decreased protein levels in adulthood, indicating impaired mitochondrial biogenesis (Fig. 1 *E* and *F*). Next, we calculated mitochondrial DNA copy numbers and deletions using the mtDNA/nDNA and *Nd1*/*Nd4* ratio at P1.5, P12.5, and 8 wk. The mtDNA/nDNA ratio was significantly reduced and the *Nd1*/*Nd4* ratio was significantly increased in *Foxp1*$^{+/-}$ striata compared to WT striata (Fig. 1*G*), supporting the impairment of mitochondrial biogenesis in the *Foxp1*$^{+/-}$ striatum.

Genes Involved in Fission and Fusion Are Dysregulated in the *Foxp1*$^{+/-}$ Striatum, Pointing to Impaired Mitochondrial Dynamics. A direct transcriptional target of Foxp1, *Pgc-1α*, showed significantly reduced protein levels in the *Foxp1*$^{+/-}$ striatum (Fig. 1*C* and *SI Appendix*, Fig. S3). Pgc-1α regulates mitochondrial dynamics by influencing dynamin-like 120-kDa protein (*Opa1*), mitofusin-1 (*Mfn1*), and mitofusin-2 (*Mfn2*)—all involved in fusion—and dynamin-1-like protein (*Drp1*) and mitochondrial fission 1 protein (*Fis1*), which are involved in fission (Fig. 2*A*). Expression of these genes was also altered in the *Foxp1*$^{+/-}$ striatum at one or more of the investigated time points (*SI Appendix*, Fig. S4).

Mfn1 protein levels, were significantly reduced at P12.5 and elevated at 8 wk in the *Foxp1*$^{+/-}$ striatum compared to WT (Fig. 2*B* and *SI Appendix*, Fig. S5*A*). Opa1 has two isoforms: L-Opa1 and S-Opa1. S-Opa1 protein expression was lower at all three time points. The increased L-Opa1/S-Opa1 ratio (Fig. 2*B* and *SI Appendix*, Fig. S5*B*) suggests disturbed *Foxp1*$^{+/-}$ mitochondrial morphology (31). Drp1 protein levels increased at P1.5 and decreased at P12.5 and 8 wk in *Foxp1*$^{+/-}$ striata (Fig. 2*C* and *SI Appendix*, Fig. S5*C*). Reversible Drp1 phosphorylation at Drp1(Ser637) blocks mitochondrial fission (32), so we measured Ser637-phosphorylated Drp1 and detected higher levels in the *Foxp1*$^{+/-}$ striatum than in the WT striatum at all three stages (Fig. 2*C* and *SI Appendix*, Fig. S5*C*). Fis1 mediates fission by recruiting Drp1 to mitochondria and also promotes mitophagy. Significantly elevated Fis1 protein levels in *Foxp1*$^{+/-}$ striata at all examined stages indicate increased mitochondrial fission (Fig. 2*C* and *SI Appendix*, Fig. S5*D*). However, Drp1 must be recruited from the cytoplasm to the mitochondrial surface to mediate the mitochondrial fission (33). Higher Drp1 expression was detected in the cytosolic fraction at P12.5 and 8 wk (*SI Appendix*, Fig. S5*E*), suggesting decreased fission in the *Foxp1*$^{+/-}$ striatum.

Mitophagy Is Increased in the *Foxp1*$^{+/-}$ Striatum. Damaged or excess mitochondria are eliminated by mitophagy. The microtubule-associated protein 1A/1B-light chain 3I (LC3I) is conjugated to phosphatidylethanolamine to form LC3II, a structural protein in autophagosomal membranes. We measured both LC3 isoform expressions to monitor autophagy and autophagic cell death. Western blot analysis showed that LC3A/BII expression was significantly higher in *Foxp1*$^{+/-}$ than WT tissue at all three time points (Fig. 2*D* and *SI Appendix*, Fig. S6*A*). Mitophagy in primary striatal neurons was assessed by quantifying the colocalization of Mitotracker and Lysotracker (34). *Foxp1*$^{+/-}$ neurons exhibited increased mitophagy by ∼95% compared to WT (Fig. 2*E*). The Pink-Parkin pathway orchestrates the removal of damaged mitochondria in mitophagy. In line with this, we observed significantly elevated *Pink1* mRNA and its protein as well as Parkin protein expression in *Foxp1*$^{+/-}$ striatal tissue, indicating increased mitophagy (*SI Appendix*, Fig. S6 *B* and *C*).

Mitochondrial Dysfunction and Excessive Oxidative Stress in the *Foxp1*$^{+/-}$ Striatum. Proper mitochondrial dynamics, biogenesis, and mitophagy are essential for the maintenance of mitochondrial homeostasis and function. As mitochondria supply energy by generating metabolites and adenosine triphosphate (ATP) via tricarboxylic acid cycle (TCA) and oxidative phosphorylation (OXPHOS), we measured adenosine compounds (ATP, adenosine diphosphate [ADP], adenosine monophosphate [AMP], nicotinamide adenine dinucleotide [NAD], nicotinamide adenine dinucleotide-hydrogen [NADH], nicotinamide adenine dinucleotide phosphate [NADPH], 5′-methylthioadenosine, adenosine, S-adenosylmethionine) in primary striatal neurons. *Foxp1*$^{+/-}$ cells

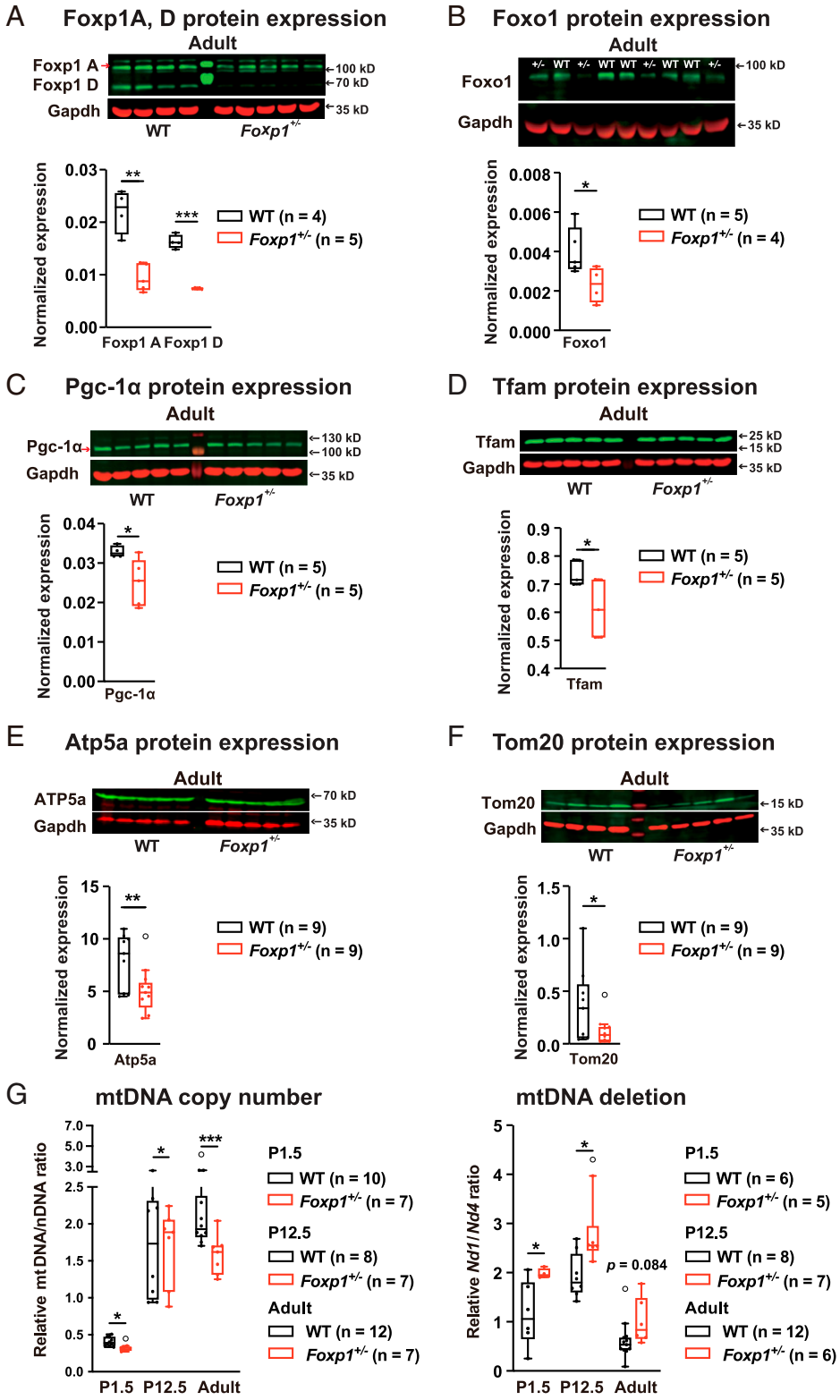

Fig. 1. Mitochondrial biogenesis is altered in the *Foxp1*$^{+/-}$ striatum. (*A*) The expression of Foxp1 isoform A and D were quantified in adult WT and *Foxp1*$^{+/-}$ striatal tissue by Western blot. At the age of 8 wk Foxp1 A was reduced by ∼57% and Foxp1 D by ∼55% in *Foxp1*$^{+/-}$ mice compared to WT animals. (*B*) Foxo1 protein was reduced by ∼42% in adult *Foxp1*$^{+/-}$ tissue, (*C*) Pgc-1α by ∼24%, and (*D*) Tfam by ∼17%. (*E* and *F*) Atp5a and Tom20 were decreased by ∼33% and ∼64%, respectively, compared with WT mice at adult stage. (*G*) Mitochondrial copy number and mtDNA deletion were evaluated by quantitative real-time PCR. The mtDNA/nDNA ratio was calculated by normalizing the expression of *D-loop*, *16sRNA*, and *Nd1* to *Hk2* and *B2m*. mtDNA/nDNA ratios were reduced in *Foxp1*$^{+/-}$ tissue at all three stages, indicating a decreased mitochondrial copy number. The *Nd1/Nd4* ratio was elevated in the *Foxp1*$^{+/-}$ striatum at P1.5 and P12.5, indicating increased mtDNA deletions. In each experiment, at least four animals per group were used, the exact number of animals is given in the figure. In the box-and-whisker plot, the boxes represent the first and third quartiles, the whiskers represent 95% CI, and the lines within the boxes are median values. Weak outliers are marked with a circle. Asterisks indicate a significant difference (*$P \leq 0.05$, **$P \leq 0.01$, ***$P \leq 0.001$); two-way ANOVA.

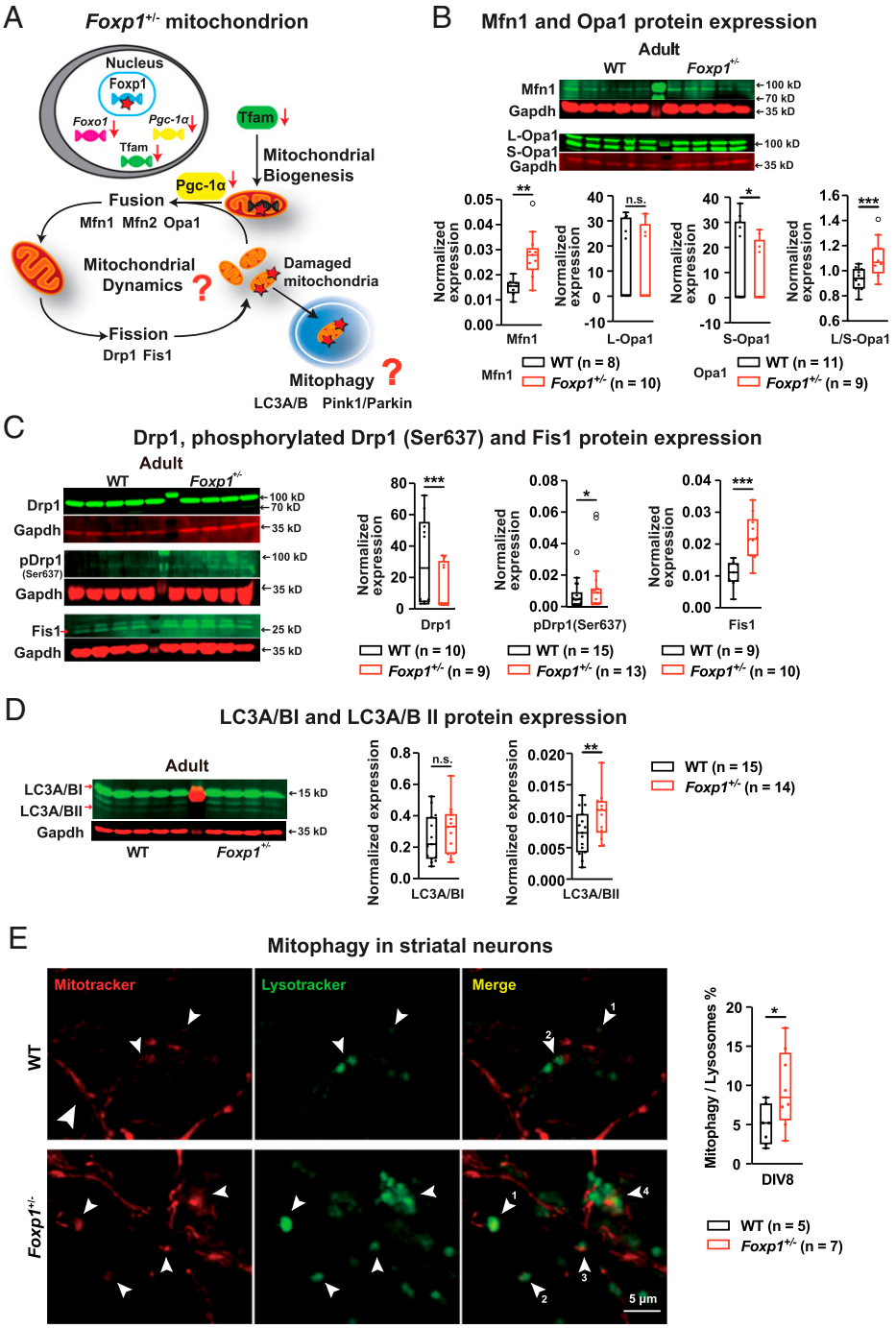

Fig. 2. The *Foxp1*$^{+/-}$ striatum displays altered mitochondrial dynamics and increased mitophagy. (*A*) Scheme illustrating alterations of the mitochondrial machinery in the *Foxp1*$^{+/-}$ striatum. Reduced Foxp1, Foxo1, Tfam, and Pgc-1α expression indicating disrupted mitochondrial biogenesis is represented by down-pointing arrows (red). Pgc-1α initiates mitochondrial dynamics by regulating genes involved in fusion (*Mfn1*, *Mfn2*, and *Opa1*) and fission (*Drp1* and *Fis1*). LC3A/B and Pink-Parkin regulate mitophagy to eliminate damaged mitochondria. (*B*) Mfn1 expression was increased by ∼89% in *Foxp1*$^{+/-}$ striata at 8 wk compared to WT tissue. Long (L)-Opa1 expression was not altered, short (S)-Opa1 expression by ∼27% at 8 wk in the *Foxp1*$^{+/-}$ striatum. Consequently, the ratio of L-Opa1/S-Opa1 was significantly increased in the *Foxp1*$^{+/-}$ striatum than in WT tissue at adult by ∼20%. (*C*) Drp1 levels were increased by ∼51% at 8 wk in *Foxp1*$^{+/-}$ animals. pDrp1 (Ser637) showed a significantly increased expression at adulthood compared to WT mice. Fis1 displayed an increased expression by ∼109% at 8 wk in the *Foxp1*$^{+/-}$ striatum. (*D*) LC3A/BI and LC3A/BII isoform expression was quantified by Western blot in striatal tissue of both genotypes. LC3A/BI expression did not differ between the genotypes; however, LC3A/BII levels were significantly increased in *Foxp1*$^{+/-}$ tissue at 8 wk. (*E*) Mitophagy was increased by ∼95% in *Foxp1*$^{+/-}$ striatal neurons at DIV8, as shown by colocalization of Mitotracker and Lysotracker staining (see arrowheads) (WT = 5 mice, 7 images, 3,441 total lysosomes; *Foxp1*$^{+/-}$ = 7 mice, 8 images, 5,037 total lysosomes). In each experiment, at least five animals per group were used, the exact number of animals is given in the figure. Weak outliers are marked with a circle. Asterisks indicate significant difference (*$P \leq 0.05$, **$P \leq 0.01$, ***$P \leq 0.001$); n.s., nonsignificant; two-way ANOVA; DIV, days in vitro.

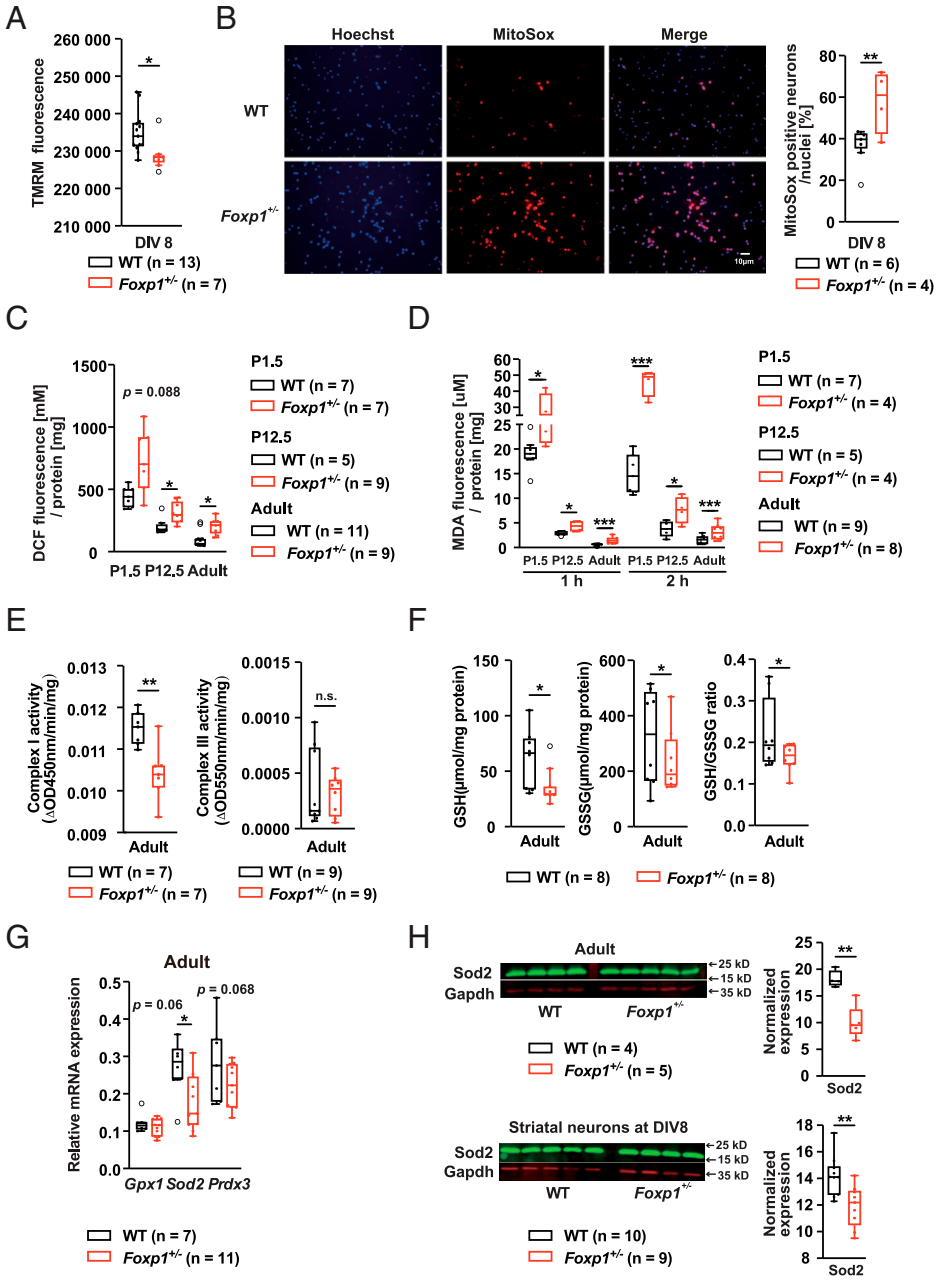

Fig. 3. The *Foxp1*$^{+/-}$ striatum exhibits mitochondrial dysfunction and increased oxidative stress. (*A*) Mitochondrial membrane potential (Δψm) was measured in primary striatal neurons of both genotypes by TMRM staining. The TMRM fluorescent signal was significantly lower in *Foxp1*$^{+/-}$ neurons compared to WT cells, indicating a lower mitochondrial membrane potential. (*B*) ROS abundance was quantified in living striatal neurons by MitoSOX Red, nuclei (blue) were stained with Hoechst 33324. *Foxp1*$^{+/-}$ cultures had ∼64% more MitoSOX-red-positive neurons than WT cultures, indicating increased amounts of ROS. (*C*) DCF detection of striatal tissue at P1.5, P12.5, and 8 wk. *Foxp1*$^{+/-}$ tissue showed increased DCF fluorescence at P12.5 and 8 wk compared to WT tissue indicating elevated ROS levels. (*D*) Measurement of lipid peroxidation in striatal tissue by malondialdehyde (MDA) fluorescence. At all three stages, MDA fluorescence was significantly increased in *Foxp1*$^{+/-}$ tissue after 1 h and 2 h of incubation compared with WT tissue. (*E*) Complex I and III activity in the adult WT and *Foxp1*$^{+/-}$ striatum. Complex I activity was decreased by ∼9% in *Foxp1*$^{+/-}$ tissue compared with WT, whereas complex III activity did not differ between the genotypes. (*F*) Measurement of reduced glutathione (GSH) and oxidized glutathione disulfide (GSSG). Reduced GSH is decreased by ∼40% and oxidized GSSG by ∼27% in *Foxp1*$^{+/-}$ tissue, leading to an elevated GSSG/GSH ratio by ∼25%. (*G*) mRNA expression of *Gpx1*, *Sod2*, and *Prdx3* was analyzed by quantitative real-time PCR at the age of 8 wk. *Foxp1*$^{+/-}$ striata exhibited a reduced expression of *Sod2* by ∼33% compared to WT tissue. (*H*) Sod2 protein was quantified in striatal tissue at the age of 8 wk and in primary striatal neurons (DIV8) by Western blot. Both *Foxp1*$^{+/-}$ striatum and primary neurons displayed reduced Sod2 levels by ∼45% and ∼16%, respectively, compared to WT. In *A* and *B*, at least four animals per group were investigated and at least three replicates were performed per animal. The exact number of animals used is given in the figure. Weak outliers are marked with a circle. Asterisks indicate a significant difference (*$P \leq 0.05$, **$P \leq 0.01$, ***$P \leq 0.001$); n.s., nonsignificant; two-way ANOVA; DIV, days in vitro.

exhibited increased AMP and decreased NADPH levels; all other molecules tested were not altered (*SI Appendix*, Fig. S7).

Mitochondrial membrane potential (Δψm) drives ATP generation; therefore, we compared the Δψm in WT and *Foxp1*$^{+/-}$ striatal neurons. The Δψm was lower in *Foxp1*$^{+/-}$ neurons than in WT neurons, as shown by decreased tetramethylrhodamine, methyl ester (TMRM; readily sequestered by active mitochondria) fluorescence, which indicates reduced OXPHOS in

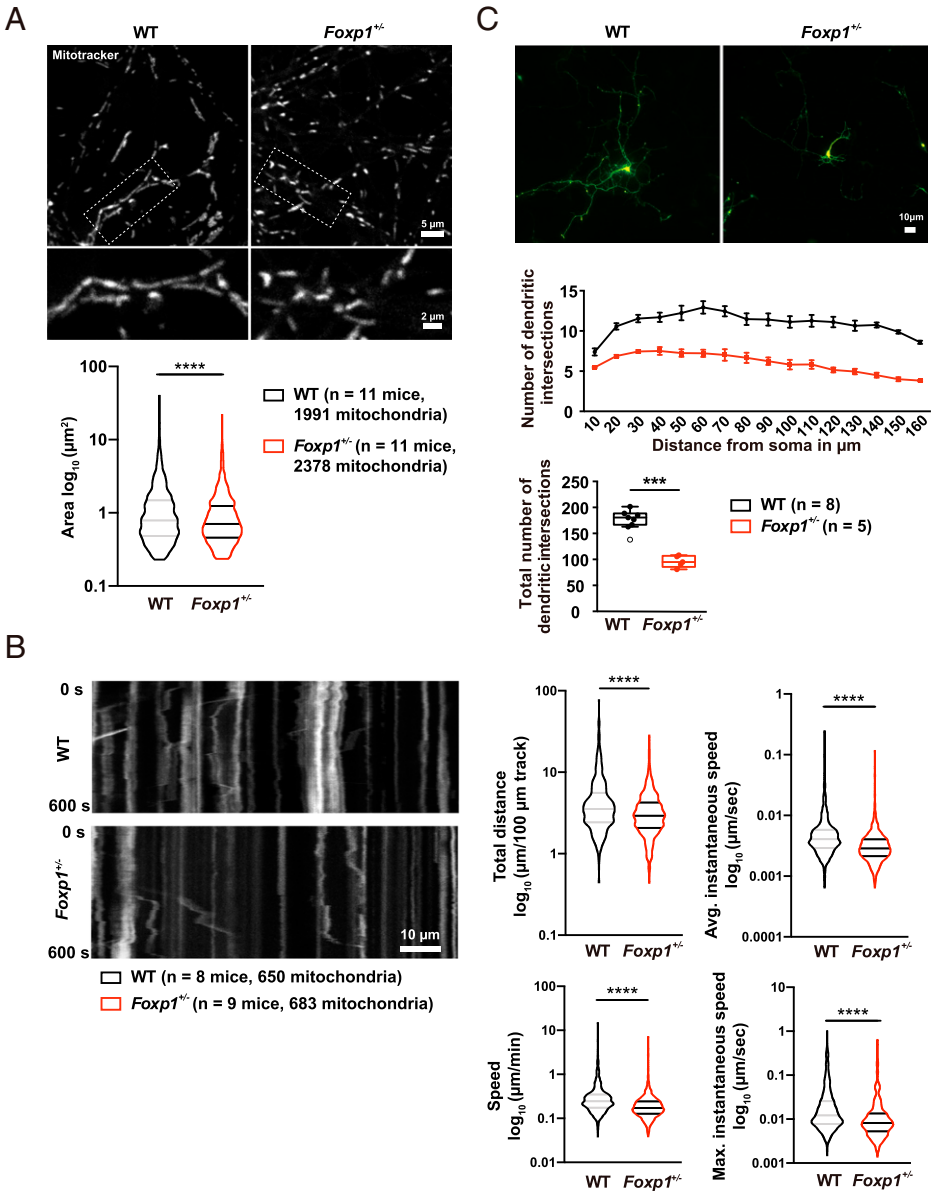

Fig. 4. *Foxp1*$^{+/-}$ striatal neurons show an altered mitochondrial structure and dynamics and dendritic arborization at DIV8. (*A*) Mitochondrial surface area was analyzed after staining with MitoTracker. There is no difference in the surface mitochondria content between genotypes (WT = 130.8 ± 23.17 µm^2 (*n* = 11 mice, 20 images); *Foxp1*$^{+/-}$ = 126.1 ± 19.92 µm^2 (*n* = 11 mice, 20 images). *Foxp1*$^{+/-}$ neurons displayed a decrease in mitochondrial surface area compared to WT cells (WT = 1.314 ± 1.777 µm^2; *Foxp1*$^{+/-}$ = 1.061 ± 1.202 µm^2). A total of 1,991 WT and 2,378 *Foxp1*$^{+/-}$ mitochondria from 11 animals each were analyzed. (*B*) Kymographs of mitochondria in neurite extensions (10 min) demonstrate altered mitochondrial movement in *Foxp1*$^{+/-}$neurons. The distance of mitochondrial movement in *Foxp1*$^{+/-}$ striatal neurons was reduced compared to WT mitochondria (WT 5.141 ± 5.823 µm/100 µm kymograph; *Foxp1*$^{+/-}$ 3.568 ± 2.693 µm/100 µm kymograph). In addition, *Foxp1*$^{+/-}$ mitochondria displayed a reduced speed as demonstrated by decreased displacement average speed (WT 0.363 ± 0.692 µm/min; *Foxp1*$^{+/-}$ 0.229 ± 0.362 µm/min), instantaneous average speed (WT 0.0059 ± 0.0113 µm/s; *Foxp1*$^{+/-}$ 0.0038 ± 0.0059 µm/s), and maximum instantaneous speed (WT 0.032 ± 0.068 µm/s; *Foxp1*$^{+/-}$ 0.018 ± 0.045 µm/s). A total of 650 WT and 683 *Foxp1*$^{+/-}$ mitochondria from 8 WT and 9 *Foxp1*$^{+/-}$ animals were analyzed. (*C*) Dendritic branching was investigated in GFP transfected primary striatal neurons by Sholl analysis. *Foxp1*$^{+/-}$ neurons show an altered morphology with significant reduction of dendritic intersections by ∼45% compared with WT neurons. In each experiment, at least five animals per group were investigated and at least three replicates were performed per animal. The exact number of animals used is given in the figure. (*A* and *B*) lines within violin plots represent the median and quartiles. Weak outliers are marked with a circle. Asterisks indicate a significant difference (***$P \leq 0.001$, ****$P \leq 0.0001$); Mann–Whitney test and two-way ANOVA was performed in the analysis of mitochondrial dynamics and Sholl analysis. DIV, days in vitro.

Foxp1$^{+/-}$ mutant neurons (Fig. 3*A*). Thus, to directly estimate the rate of OXPHOS, we quantified oxygen consumption rate (OCR), an indicator of the mitochondrial respiration, using the Seahorse metabolic flux analyzer (*SI Appendix*, Fig. S8*A*). Baseline mitochondrial respiration (*SI Appendix*, Fig. S8*B*) as well as the rate of OXPHOS (*SI Appendix*, Fig. S8*C*) were similar between *Foxp1*$^{+/-}$ mutant and WT striatal neurons. In a pathological condition, to match the increased metabolic demands, cells tend to shift their metabolic state from OXPHOS toward aerobic glycolysis (35, 36). Hence, to estimate whether such "metabolic state" shift occurred in *Foxp1*$^{+/-}$ mutant neurons, we quantified the rate of glycolysis by estimating extracellular acidification rate (ECAR) in our Seahorse metabolic flux analysis assays (*SI Appendix*, Fig. S8*D*). We

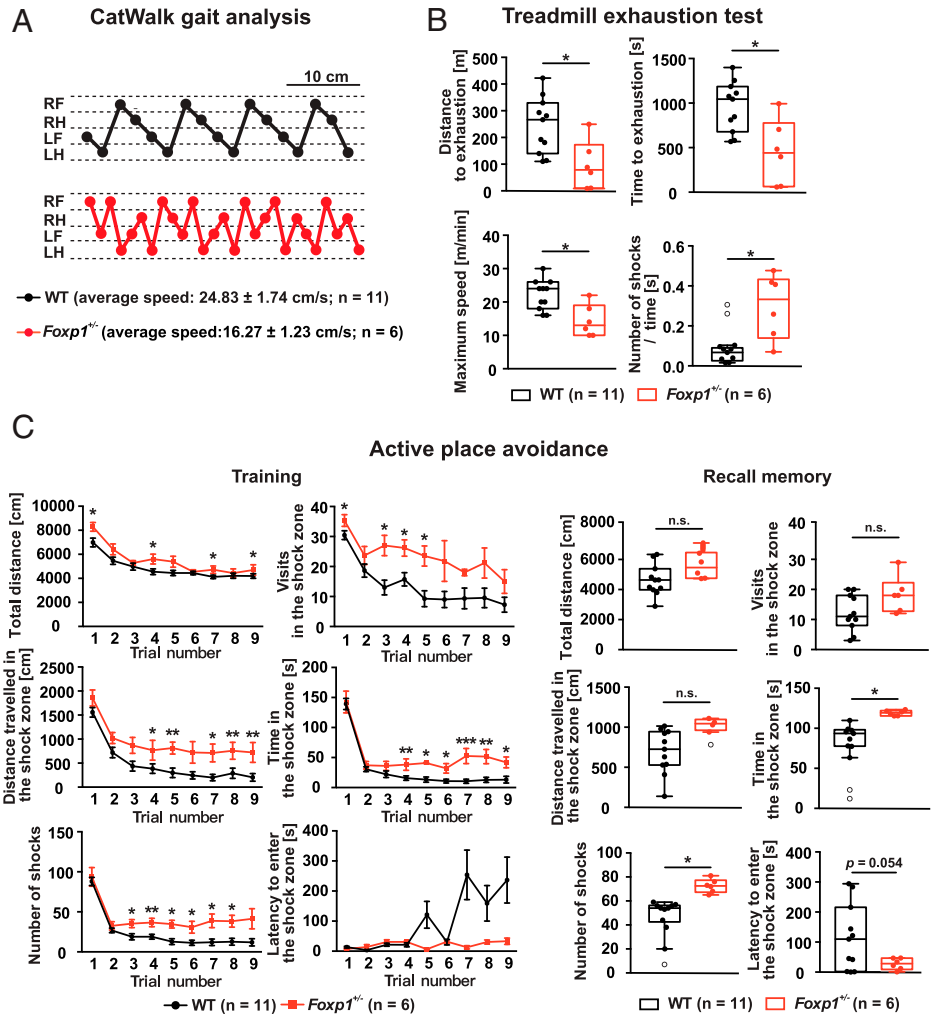

Fig. 5. *Foxp1*$^{+/-}$ mice show deficits in motor performance and cognition. (*A*) The walking pattern of WT and *Foxp1*$^{+/-}$ mice was analyzed by the CatWalk gait analysis system. *Foxp1*$^{+/-}$ mice exhibited a reduced walking speed by ~34% and their step number was significantly increased compared to WT mice. (*B*) Evaluation of endurance and muscle strength by treadmill exhaustion test. *Foxp1*$^{+/-}$ mice covered a significantly decreased distance on the treadmill (96 ± 37 m versus 245 ± 32 m), exhausted earlier (8 ± 2 min versus 16 ± 1 min), exhibited a lower maximum speed (14 ± 2 m/min versus 22 ± 1 m/min), and received significantly more electrical shocks during the same period on the treadmill than WT animals. (*C*) Active place avoidance test. On day 1 in the training phase (nine trials), *Foxp1*$^{+/-}$ mice displayed increased traveling and entered the shock zone more frequently than WT mice. In addition, they spent more time in there, covered a longer distance in the shock zone, and thus received more shocks than WT mice. On day 2, when memory was tested, *Foxp1*$^{+/-}$ mice entered the shock zone earlier, spent significantly more time in there, thus receiving ~60% more shocks than their WT littermates. In each experiment, at least six animals per group were used, the exact number of animals is given in the figure. In *C*, course diagrams represent means ± SEM. Weak outliers are marked with a circle. Asterisks indicate significant difference (*$P \leq 0.05$, **$P \leq 0.01$, ***$P \leq 0.001$); n.s., nonsignificant; three-way ANOVA. LF, left forelimb; RF, right forelimb; LH, left hindlimb; and RH, right hindlimb.

found that *Foxp1*$^{+/-}$ and WT striatal neurons performed glycolysis at a similar level (*SI Appendix*, Fig. S8*E*).

Next, we quantified ROS in living primary striatal neurons and striatal tissue. Significantly more *Foxp1*$^{+/-}$ neurons than WT neurons were stained positively with superoxide stain MitoSOX Red (Fig. 3*B*). More ROS were also detected in *Foxp1*$^{+/-}$ than in WT striatal tissue as shown by quantification of 2′, 7′-dichlorofluorescein (DCF) (Fig. 3*C*). Moreover, significantly elevated malondialdehyde formation and higher 4-hydroxynonenal levels in the *Foxp1*$^{+/-}$ striatum points to increased lipid peroxidation (Fig. 3*D* and *SI Appendix*, Fig. S9*A*). A source of elevated ROS may be mitochondrial complex I and complex III, especially under pathological conditions (37, 38). The activity of complex I was significantly reduced in the *Foxp1*$^{+/-}$ striatum, while the activity of complex III was not altered in 8-wk-old animals (Fig. 3*E*). Excessive ROS in cells are degraded by antioxidants such as reduced glutathione (GSH). *Foxp1*$^{+/-}$ tissue exhibited decreased GSH and oxidized glutathione (GSSG) levels as well as a reduced GSH/GSSG ratio, indicating significantly increased oxidative stress (Fig. 3*F*). To assess antioxidative capacity, we measured glutathione peroxidase 1 (*Gpx1*), superoxide dismutase 2 (*Sod2*), and thioredoxin-dependent peroxide reductase (*Prdx3*). We detected reduced *Gpx1* and *Prdx3* expression at P1.5 and P12.5 and reduced *Sod2* levels at P12.5 and 8 wk in the *Foxp1*$^{+/-}$ striatum (Fig. 3*G* and *SI Appendix*, Fig. S9*B*). Elevated ROS at P12.5 and 8 wk in *Foxp1*$^{+/-}$ tissue suggests that *Sod2* might play the major role in ROS accumulation. Sod2 protein analysis confirmed this, showing strongly reduced expression in striatal primary *Foxp1*$^{+/-}$ neurons at 8 days of in vitro differentiation (DIV8) and in P1.5 and 8-wk-old *Foxp1*$^{+/-}$ animals (Fig. 3*H* and *SI Appendix*, Fig. S9*C*).

Increased oxidative stress triggers apoptosis (39, 40). To investigate apoptosis, we measured mitochondrial cytochrome *c* release, which is linked to early stages of apoptosis.

Comparable to the analysis of ROS, cytochrome *c* levels in the cytosolic fraction did not differ at P1.5, but were significantly elevated in *Foxp1*$^{+/-}$ tissue at P12.5 and 8 wk (*SI Appendix*, Fig. S10*A*). We further analyzed apoptosis by active (cleaved) caspase-3 immunostaining and by terminal deoxynucleotidyl transferase dUTP nick end labeling (TUNEL) assay at the three developmental time points and quantified active caspase-3 in the adult striatum by Western blot. However, an increased rate of apoptosis in the *Foxp1*$^{+/-}$ striatum was not detected (*SI Appendix*, Figs. S10 *B* and *C* and S11). Taken together, these results suggest that *Foxp1*$^{+/-}$ neurons are able to maintain their metabolic state without switching between OXPHOS and glycolysis, but at a price of increased mitochondrial stress and ROS generation.

Mitochondrial Structure, Motility, and Dendritic Arborization Are Altered in *Foxp1*$^{+/-}$ Striatal Neurons. Mitochondrial stress and excessive ROS generation can lead to breakdown of mitochondrial network structure and influence the mitochondrial motility. To evaluate mitochondrial structure and dynamics, we stained neurons of both genotypes by using Mitotracker and performed live-cell two-photon microscopy. Semiautomated segmentation of the mitochondria revealed that *Foxp1*$^{+/-}$ neurons had a ∼19.2% decrease in mitochondrial surface area compared to WT neurons (Fig. 4*A*). Moreover, *Foxp1*$^{+/-}$ neurons revealed a reduced proportion of elongated mitochondria, a sign of mitochondrial stress (*SI Appendix*, Fig. S5 *F* and *G*). To track mitochondrial movement over time, we created kymographs using a semiautomatic algorithm in an image analysis software, ICY. *Foxp1*$^{+/-}$ mitochondria displayed a consistent decrease in the total distance moved and the average speed of motility compared to WT mitochondria (Fig. 4*B*). We hypothesized that increased ROS and alterations in the mitochondrial network dynamics might impair neuronal morphology. Therefore, we examined the dendritic arbor complexity of GFP-transfected WT and *Foxp1*$^{+/-}$ striatal neurons by Sholl analysis after 8 d of differentiation, and found ∼45% fewer dendritic intersections in *Foxp1*$^{+/-}$ neurons than in WT neurons (Fig. 4*C*). Hence, our results suggest that ongoing mitochondrial stress impairs mitochondrial structural dynamics and affects neuronal arborization.

***Foxp1*$^{+/-}$ Mice Exhibit Deficits in Motor Performance and in Learning and Memory.** Striatal dysfunction probably contributes to the pathology of FOXP1 deficiency in a fundamental way. Since the striatum plays an essential role in motor control and motor learning, we investigated gait, coordination, and endurance in *Foxp1*$^{+/-}$ mice. The CatWalk gait analysis revealed a slow, hesitant walking pattern together with an increased number of steps, altered step characteristics, and gait variability as well as disrupted interpaw coordination compared with WT mice (Fig. 5*A* and *SI Appendix*, Table S1). In the treadmill exhaustion test, *Foxp1*$^{+/-}$ mice stopped running after 8 ± 2 min and covered a distance of 96 ± 37 m compared with WT mice, which stopped running after 16 ± 1 min and covered a distance of 245 ± 32 m. *Foxp1*$^{+/-}$ mice also ran significantly slower than WT mice did (maximum speed 14 ± 2 m/min in *Foxp1*$^{+/-}$ mice compared with 22 ± 1 m/min in WT mice) (Fig. 5*B*).

We also tested active place avoidance because the striatum as a major component of the basal ganglia circuitry affects emotional and spatial learning (41, 42). In this test, *Foxp1*$^{+/-}$ mice could not avoid the shock zone. They entered the shock zone significantly more often, stayed there significantly longer, and covered a greater distance therein during the training phase, receiving more shocks than WT littermates did (Fig. 5*C* and Movies S1 and S2). The learning deficiency was confirmed in the following recall memory test. *Foxp1*$^{+/-}$ mice spent more time in the shock zone and received more shocks than WT animals (Fig. 5*C* and Movies S3 and S4).

Discussion

In this study, we show that *Foxp1* haploinsufficiency in mice leads to similar deficits in cognitive and motor function as reported in individuals with FOXP1 syndrome, and that mitochondrial dysfunction and oxidative stress is associated with these deficits.

Genes that regulate mitochondrial biogenesis and metabolism (*Foxo1*, *Pgc-1α*, *Nrf1*, *Nrf2*, *Tfam*, *Pparα*, and *Pparγ*) were all shown to be dysregulated in the *Foxp1*$^{+/-}$ striatum. A comparison of these data to Nestin-Cre (*Foxp1*$^{-/-}$) mice with a complete loss of *Foxp1* in the nervous system (12) and to mice with a complete loss of *Foxp1* in both D1- and D2-medium spiny neurons (MSNs) or D2-MSNs alone (15) revealed that reduced *Foxp1* expression in *Foxp1*$^{+/-}$ mice affects gene expression differently than the complete loss of *Foxp1* does. An example is *Pgc-1α* (28, 43), regulated by Foxo1, which is a transcriptional coactivator and master regulator of mitochondrial biogenesis. Reduced Foxo1 and Pgc-1α levels in the *Foxp1*$^{+/-}$ striatum were also detected by RNA sequencing (RNA-seq) (9). *Pgc-1α* coactivates nuclear respiratory factor 2 (*Nrf2*), and together with Nrf2 coactivates *Nrf1* (44). In turn, Pgc-1α and Nrf1/2 regulate *Tfam* transcription in response to increased mitochondrial biogenesis (45). Most likely a reduced *Pgc-1α* transcriptional activation by Foxo1 in *Foxp1*$^{+/-}$ tissue is responsible for the decreased Tfam expression, a protein regulating mitochondrial genome replication and transcription (46, 47). Disrupted mitochondrial biogenesis was also shown by altered mtDNA/nDNA ratios, elevated *Nd1*/*Nd4* ratios, and reduced Atp5a as well as Tom20 levels in the *Foxp1*$^{+/-}$ striatum.

Pgc-1α also controls the delicate equilibrium between fusion and fission in mitochondria and stimulates *Mfn1* (48), which, together with Mfn2, regulates the fusion of outer mitochondrial membranes. The adult *Foxp1*$^{+/-}$ striatum reveals a reduced *Mfn1* mRNA expression, whereas Mfn1 protein levels are significantly increased. This suggests a compensatory upregulation of *Mfn1* translation in the adult *Foxp1*$^{+/-}$ striatum, which might enhance outer mitochondrial fusion. Since L- and S-Opa1 cooperate in mediating the fusion of inner mitochondrial membranes by influencing the pore opening efficiency (31, 49), we assume that reduced S-Opa1 may lead to inefficient and slow fusion of inner mitochondrial membrane as well as disrupted mitochondrial structure and energetics. In addition, Drp1 (which activates fission) was reduced, whereas phosphorylated-Ser637 Drp1 (which blocks fission) (32, 50) was increased in the *Foxp1*$^{+/-}$ striatum, pointing to reduced mitochondrial fission. Thus, we conclude that disrupted mitochondrial dynamics might impair cellular energy supply and induce cellular stress.

Mitochondrial biogenesis and dynamics as well as the removal of damaged mitochondria are essential for mitochondrial function. Interestingly, we found that Fis1 expression is increased in the *Foxp1*$^{+/-}$ striatum, and elevated Fis1 has been associated with mitochondrial fragmentation and autophagosome formation (51). LC3A/BII are microtubule-associated proteins essential for autophagosomes assembly (52). Elevated LC3A/BII expression indicates increased autophagy in the *Foxp1*$^{+/-}$ striatum. However, increased mitophagy was also noted, supported by increased Pink1 and Parkin, two proteins promoting mitophagy upon loss of mitochondrial membrane potential (53). Strikingly, mitochondrial membrane potential was reduced in *Foxp1*$^{+/-}$ striatal cells, which may influence ATP production. However, only AMP, a sensitive indicator of energy consumption, was altered. Elevated AMP/ATP ratios in *Foxp1*$^{+/-}$ neurons suggest a compromised energy status in the *Foxp1*$^{+/-}$ striatum (54).

The increased occurrence of ROS in the *Foxp1*$^{+/-}$ striatum is based on two different aspects: A reduced complex I activity with elevated ROS production, and a decreased degradation

due to reduced Sod2 and GSH levels. *Sod2* is a direct transcriptional target of Foxo1 (55), whereas GSH production is regulated by glutathione reductase, which depends on NADPH as an indispensable cofactor (56). As NADPH is an essential electron donor, decreased NADPH levels indicate a diminished reducing force for redox balance in the *Foxp1*$^{+/-}$ striatum (57). However, the increased ROS accumulation does not result in cell death; rather in cell injury, morphological changes and cellular function deficits (58). In line with this, we observed a premature dendritic morphology of striatal neurons in *Foxp1*$^{+/-}$ animals. Altered dendritic growth and/or maintenance disrupt neural network function, ultimately leading to social and cognitive impairment. Indeed, impaired connectivity between the higher-order association areas is a major defect in ASD (59) and seems to hold true for FOXP1 syndrome as well.

Mitochondrial dysfunction is found more frequently in individuals with ASD than in the general population, but seems to affect only a subset of individuals with ASD (19). To define this subgroup, expression and regulation of mitochondria-related genes can be tested. Some ASD-associated risk genes (*SLC25A12*, *MTX2*, *NEF*, *SLC25A27*, *SHANK3*, and *SCO2*) have already been proposed to play a role in mitochondrial function (60–62). As Foxp1 is expressed in many tissues apart from brain, mitochondrial defects in FOXP1 deficiency may also occur in these tissues. This corresponds well with the understanding that FOXP1 syndrome and ASD is not only a central nervous system disorder but also causes muscular, gastrointestinal, endocrine, and immune deficiencies (19, 63). FOXP1 deficiency, therefore, defines one subgroup of ASD individuals affected by mitochondrial dysfunction.

Mitochondrial dysfunction and increased oxidative stress can interplay and activate components of pathways regulating autophagy, apoptosis, and inflammation. These defects will inevitably affect all areas of cognition and motor function that rely on the basal ganglia circuitry. Moreover, mitochondrial function plays an important role in neurogenesis, synaptic plasticity, and neurotransmission (16–18). Very interesting in this context is the finding that disrupted mitochondrial activity cause GABA sequestration in mitochondria, reducing GABAergic signaling in the striatum, and resulting in social deficits (64). In this respect, we conclude that mitochondrial dysfunction does not only contribute to the pathology of FOXP1 syndrome, but may also provide the impetus for the development of this disorder.

Our finding that mitochondrial function is disrupted in the *Foxp1*$^{+/-}$ striatum may also be relevant to Huntington's disease (HD). This neurodegenerative disorder is characterized by the degeneration of GABAergic medium spiny neurons and mitochondrial dysfunction (65, 66), but the molecular mechanism by which mutant Huntingtin affects mitochondrial function remains elusive. Strikingly, FOXP1 is down-regulated in HD individuals and mouse models of HD (67, 68). Elevating Foxp1 expression protects striatal and cortical neurons from death caused by mutant Huntingtin. Conversely, *Foxp1* knockdown promotes death in healthy neurons, indicating a neuroprotective function for Foxp1 (67). This suggests that the reduced FOXP1 expression in HD contributes to mitochondrial dysfunction. Moreover, PGC-1α is also down-regulated in animal models and individuals with HD (69). In contrast, up-regulation of Pgc-1α expression prevented mitochondrial dysfunction and provided neuroprotection in the transgenic HD striatum (70), suggesting that stimulating PGC-1α function may also be beneficial in FOXP1 deficiency.

The striatum plays a vital role in the coordination of motor and cognitive information from diverse brain regions into meaningful behavioral output (15). Approximately 95% of the striatal cells are Foxp1-expressing medium spiny neurons, which, at least in vitro upon current injection spike at a higher firing rate (50 to 60 Hz) than pyramidal neurons (71, 72). Under standard recording conditions in vivo, medium spiny neurons exhibit sparse firing, but up states and subthreshold depolarization may well contribute to significant calcium influx (73). Thus, it may well be that these properties make medium spiny neurons prone to a higher energy demand and neuronal vulnerability. Considering that the striatum is strongly affected by Foxp1 deficiency, mitochondrial dysfunction in the striatum presumably plays a key role in the pathogenesis of FOXP1 syndrome.

Motor performance depends on proper muscle function, which is controlled by the striatum and spinal motor neurons. We have previously shown that conditional deletion of *Foxp1* in the central and peripheral nervous system leads to severe striatal degeneration (12); Foxp1 also plays a crucial role in the columnar organization of spinal motor neurons (74). Furthermore, muscular malfunction leads to achalasia and altered colon motility in *Foxp1*$^{+/-}$ mice (10) and gastrointestinal problems in patients (2). Our report on reduced muscle strength as well as disrupted gait and coordination in *Foxp1*$^{+/-}$ mice, pointing to hypotonia and motor dysfunction, closely mirrors the phenotype of individuals with FOXP1 deficiency (11). Impaired cognitive function is one of core features in FOXP1 syndrome. It was recently shown that output of the basal ganglia via the substantia nigra pars reticulata (SNr) gates active avoidance (42), and that the striatum plays an important role in this by regulating SNr cell activity. The complete loss of Foxp1 in the striatum leads to severe morphological and behavioral disruptions (12). Apart from the striatum, cognitive function is also dependent on the proper expression of Foxp1 in the pyramidal neurons of the neocortex and the CA1/CA2 subfields of the hippocampus (13, 14). Therefore, both alterations in the basal ganglia and corticohippocampal circuitry probably contribute to the deficits in learning and memory that we report here in *Foxp1*$^{+/-}$ mice.

In conclusion, mitochondrial dysfunction and oxidative stress in the striatum may explain the behavioral and motor deficits seen in mice and individuals with FOXP1 deficiency and provide an insight into the pathomechanisms underlying FOXP1 syndrome. Further studies, using cell type- and region-specific deletion or replenishment of Foxp1 are needed to determine whether defects in FOXP1 syndrome are restricted to the striatum or whether mitochondrial dysfunctions in other tissues also contribute to its pathology. Current medical interventions for FOXP1 syndrome and autism are not aimed at improving mitochondrial function. Strategies targeting dysregulated proteins involved in mitochondrial function, electron transport chain, or antioxidants may therefore offer new therapy options.

Methods and Materials

Animals. *Foxp1*$^{+/-}$ mice (8) were backcrossed with C57BL/6J mice for at least 12 generations to obtain congenic animals. Mice were kept in a specific pathogen-free biomedical animal facility under a 12-h light-dark cycle and given ad libitum access to water and food. All procedures were conducted in compliance with the NIH Guidelines for the Care and Use of Laboratory Animals and were in accordance with the German Animal Protection Law (TierSCHG). The day of birth was considered as postnatal day (P) 0.5. Animal studies were approved by the Governmental Council Karlsruhe, Germany (license Nos.: 35.9185.81-G-100/16 and 35.9185.81-G-102/16).

Behavioral Analysis. CatWalk gait analysis, treadmill exhaustion test, and active place avoidance were performed as described in *SI Appendix, Methods and Materials*.

Analysis of mRNA and protein expression levels as well as the calculation of mitochondrial DNA copy number and DNA deletion are described in *SI Appendix, Methods and Materials*. Primer sequences are listed in *SI Appendix*, Table S2, primary and secondary antibodies in *SI Appendix*, Table S3.

Detection of Mitochondrial Membrane Potential. Mitochondrial membrane potential of primary neurons was measured by fluorescent staining of tetramethylrhodamine methyl ester (Image-iT TMRM reagent, Thermo Fisher Scientific) according to the manufacturer's instructions.

Measuring ROS in Striatal Tissue. Striatal ROS was marked by 2′ 7′-dichlorodihydrofluorescein diacetate (Molecular Probes H2DCFDA (H2-DCF, DCF), Thermo Fisher Scientific) as previously described (75) and assessed by DS-11 Series Spectrophotometer/Fluorometer (DeNovix Inc.).

Detection of Lipid Peroxidation Products. Lipid peroxidation products were analyzed in striatal tissue using the Bioxytech LPO-586 kit (OxisResearch) according to the manufacturer's instructions. The tissue was homogenized in PBS-containing butylated hydroxytoluene (BHT) to prevent sample oxidation during homogenization.

Analysis of GSH and GSSG. Striatal tissue (20 mg) was homogenized with a Dounce homogenizer in phosphate-buffered saline (PBS)/0.5% Nonidet P-40. Supernatant was collected and performed on a TCA/$NaHCO_3$ deproteinization until pH equals 4 to 6. The deproteinized and neutralized supernatant was used for determining reduced GSH, total GSH, and oxidized GSSG as well as GSSG/GSH ratio was calculated as manufacturer's instructions (GSH/GSSG Ratio Detection Assay Kit, No. ab138881, Abcam).

Staining of Mitochondrial Superoxide in Living Cells. Superoxides were visualized by MitoSOX Red reagent (Thermo Fisher Scientific) according to the manufacturer's instructions. In brief, primary striatal neurons were stained with 100 nM MitoSOX Red reagent for 30 min at 37 °C and examined by the automated inverted microscope DMI4000B (Leica Camera AG).

Analysis of Mitochondrial Dynamics, Mitophagy, and Morphology. For structural analyses striatal neurons at DIV8 were incubated with MitoTracker Red CMXRos (Cat. No. M7512, Thermo Fisher Scientific), and for mitophagy quantification with Mitotracker plus Lysotracker green (Cat. No. L7526, Thermo Fisher Scientific) (34). Live-cell imaging was performed using a custom built two-photon microscope (Bergamo II, Thorlabs) using a Nikon NIR, 60× 1.0 numerical aperture (NA) objective (details in *SI Appendix, Methods and Materials*). The total number of lysosomes was obtained by Ilastik segmentation and further arivis Vision4D (v3.4) three-dimensional (3D) reconstruction. Mitophagy was measured by the ratio of Mitotracker/Lysotracker colocalization events to the total number of lysosomes. To analyze mitochondrial dynamics, kymographs were generated from the time series images using the Icy Kymograph Tracker tool (version 2.1.2.0) (76, 77). To analyze mitochondrial structure, single frame images were segmented with Ilastik (78) and the surface area was measured with the Region Properties MATLAB function (Mathworks, 2020a). Mitochondrial circularity was measured by ImageJ Analyze Particles tool.

Isolation of mitochondria, primary striatal neuron culture, Sholl analysis, coimmunoprecipitation (Co-IP), immunofluorescence, cellular adenosine compound, complex I and III activities, TUNEL assay, measurement of cytochrome *c* release, determination of the OCR and ECAR were performed using standard protocols (*SI Appendix, Methods and Materials*).

Statistics. Mice were randomly assigned to tests and investigators were blinded to genotypes. IBM SPSS Statistics 25 and Microsoft Office Excel software were used to analyze primary data. Outliers were determined via IBM SPSS Statistics 25 and strong outliers (≥3 SDs above mean) were excluded from further analysis. All data were checked for normal distribution via the Kolmogorov–Smirnov and Shapiro–Wilk test. Two-way ANOVA was performed with the litter as a second factor. In the analysis of mitochondrial dynamics, Mann–Whitney test was applied. P values of ≤0.05 were considered significant.

Data Availability. All study data are included in the article and/or supporting information.

ACKNOWLEDGMENTS. We acknowledge the expert advice of Dr. Claudia Pitzer and Barbara Kurpiers from the Interdisciplinary Neurobehavioral Core Unit, and thank the Metabolomics Core Technology Platform of the Excellence cluster "CellNetworks" (University of Heidelberg) (Deutsche Forschungsgemeinschaft [DFG] Grant ZUK 40/2010-3009262) for support. We also thank Prof. Dr. Stephan Herzig at the Joint Universitätsklinikum Heidelberg-Institute for Diabetes and Cancer Translational Diabetes Program for the use of their Seahorse Analyzer. The data storage service SDS@hd, supported by the Ministry of Science, Research, and the Arts Baden-Württemberg and the DFG through Grant INST 35/1314-1, is gratefully acknowledged. We also thank Prof. Matias Simons and Dr. Carlos Bas Orth for providing Lysotracker Green DND-26 and antibodies. We are grateful to Dr. Rolf Sprengel, Institute for Anatomy and Cell Biology and Max Planck Institute for Medical Research, Heidelberg and Dr. Yu-Chao and Prof. Hannah Monyer, Department of Clinical Neurobiology, Heidelberg, as well as Dr. Yuting Ong, Prof. Beate Niesler, Dr. Claire Bacon, and Beatrix Startt for helpful comments. We acknowledge financial support from the China Scholarship Council (Scholarship No. 201708230108) to J.W., the Chica and Heinz Schaller Foundation to A.A., and the Humboldt Foundation to R.L.S. G.A.R. is a member of the CellNetworks Cluster of Excellence (EXC 81), Interdisciplinary Center for Neurosciences, and the Center of Rare Disease.

1. D. Horn *et al.*, Identification of FOXP1 deletions in three unrelated patients with mental retardation and significant speech and language deficits. *Hum. Mutat.* **31**, E1851–E1860 (2010).
2. P. M. Siper *et al.*, Prospective investigation of FOXP1 syndrome. *Mol. Autism* **8**, 57 (2017).
3. F. K. Satterstrom *et al.*; Autism Sequencing Consortium; iPSYCH-Broad Consortium, Large-scale exome sequencing study implicates both developmental and functional changes in the neurobiology of autism. *Cell* **180**, 568–584.e23 (2020).
4. S. Li, J. Weidenfeld, E. E. Morrisey, Transcriptional and DNA binding activity of the Foxp1/2/4 family is modulated by heterotypic and homotypic protein interactions. *Mol. Cell. Biol.* **24**, 809–822 (2004).
5. E. Mendoza, C. Scharff, Protein-protein interaction among the FoxP family members and their regulation of two target genes, *VLDLR* and *CNTNAP2* in the zebra finch song system. *Front. Mol. Neurosci.* **10**, 112 (2017).
6. C. S. Lai, S. E. Fisher, J. A. Hurst, F. Vargha-Khadem, A. P. Monaco, A forkhead-domain gene is mutated in a severe speech and language disorder. *Nature* **413**, 519–523 (2001).
7. M. Co, A. G. Anderson, G. Konopka, FOXP transcription factors in vertebrate brain development, function, and disorders. *Wiley Interdiscip. Rev. Dev. Biol.* **9**, e375 (2020).
8. B. Wang *et al.*, Foxp1 regulates cardiac outflow tract, endocardial cushion morphogenesis and myocyte proliferation and maturation. *Development* **131**, 4477–4487 (2004).
9. D. J. Araujo *et al.*, FoxP1 orchestration of ASD-relevant signaling pathways in the striatum. *Genes Dev.* **29**, 2081–2096 (2015).
10. H. Fröhlich *et al.*, Gastrointestinal dysfunction in autism displayed by altered motility and achalasia in *Foxp1* $^{+/-}$ mice. *Proc. Natl. Acad. Sci. U.S.A.* **116**, 22237–22245 (2019).
11. I. Meerschaut *et al.*, *FOXP1*-related intellectual disability syndrome: A recognisable entity. *J. Med. Genet.* **54**, 613–623 (2017).
12. C. Bacon *et al.*, Brain-specific *Foxp1* deletion impairs neuronal development and causes autistic-like behaviour. *Mol. Psychiatry* **20**, 632–639 (2015).
13. N. Usui *et al.*, Foxp1 regulation of neonatal vocalizations via cortical development. *Genes Dev.* **31**, 2039–2055 (2017).
14. D. J. Araujo *et al.*, Foxp1 in forebrain pyramidal neurons controls gene expression required for spatial learning and synaptic plasticity. *J. Neurosci.* **37**, 10917–10931 (2017).
15. A. G. Anderson, A. Kulkarni, M. Harper, G. Konopka, Single-cell analysis of Foxp1-driven mechanisms essential for striatal development. *Cell Rep.* **30**, 3051–3066.e7 (2020).
16. O. Kann, R. Kovács, Mitochondria and neuronal activity. *Am. J. Physiol. Cell Physiol.* **292**, C641–C657 (2007).
17. M. Khacho, R. S. Slack, Mitochondrial dynamics in the regulation of neurogenesis: From development to the adult brain. *Dev. Dyn.* **247**, 47–53 (2018).
18. Z. Li, K. Okamoto, Y. Hayashi, M. Sheng, The importance of dendritic mitochondria in the morphogenesis and plasticity of spines and synapses. *Cell* **119**, 873–887 (2004).
19. D. A. Rossignol, R. E. Frye, Mitochondrial dysfunction in autism spectrum disorders: A systematic review and meta-analysis. *Mol. Psychiatry* **17**, 290–314 (2012).
20. A. Valiente-Pallejà *et al.*, Genetic and clinical evidence of mitochondrial dysfunction in autism spectrum disorder and intellectual disability. *Hum. Mol. Genet.* **27**, 891–900 (2018).
21. A. K. Le Fevre *et al.*, FOXP1 mutations cause intellectual disability and a recognizable phenotype. *Am. J. Med. Genet. A.* **161A**, 3166–3175 (2013).
22. R. N. Krajeski, A. Macey-Dare, F. van Heusden, F. Ebrahimjee, T. J. Ellender, Dynamic postnatal development of the cellular and circuit properties of striatal D1 and D2 spiny projection neurons. *J. Physiol.* **597**, 5265–5293 (2019).
23. R. T. Peixoto, W. Wang, D. M. Croney, Y. Kozorovitskiy, B. L. Sabatini, Early hyperactivity and precocious maturation of corticostriatal circuits in *Shank3B*$^{(-/-)}$ mice. *Nat. Neurosci.* **19**, 716–724 (2016).
24. Y. Zou *et al.*, Forkhead box P1 (FOXP1) transcription factor regulates hepatic glucose homeostasis. *J. Biol. Chem.* **290**, 30607–30615 (2015).
25. Z. Cheng *et al.*, Foxo1 integrates insulin signaling with mitochondrial function in the liver. *Nat. Med.* **15**, 1307–1311 (2009).
26. D. Lettieri-Barbato *et al.*, FoxO1 localizes to mitochondria of adipose tissue and is affected by nutrient stress. *Metabolism* **95**, 84–92 (2019).
27. Z. Gan, T. Fu, D. P. Kelly, R. B. Vega, Skeletal muscle mitochondrial remodeling in exercise and diseases. *Cell Res.* **28**, 969–980 (2018).
28. P. Puigserver *et al.*, Insulin-regulated hepatic gluconeogenesis through FOXO1-PGC-1α interaction. *Nature* **423**, 550–555 (2003).
29. B. Sheng *et al.*, Impaired mitochondrial biogenesis contributes to mitochondrial dysfunction in Alzheimer's disease. *J. Neurochem.* **120**, 419–429 (2012).

30. R. Ventura-Clapier, A. Garnier, V. Veksler, Transcriptional control of mitochondrial biogenesis: The central role of PGC-1alpha. *Cardiovasc. Res.* **79**, 208–217 (2008).
31. H. Lee, S. B. Smith, Y. Yoon, The short variant of the mitochondrial dynamin OPA1 maintains mitochondrial energetics and cristae structure. *J. Biol. Chem.* **292**, 7115–7130 (2017).
32. A. Jahani-Asl, R. S. Slack, The phosphorylation state of Drp1 determines cell fate. *EMBO Rep.* **8**, 912–913 (2007).
33. B. Westermann, Mitochondrial fusion and fission in cell life and death. *Nat. Rev. Mol. Cell Biol.* **11**, 872–884 (2010).
34. S. Rodriguez-Enriquez, I. Kim, R. T. Currin, J. J. Lemasters, Tracker dyes to probe mitochondrial autophagy (mitophagy) in rat hepatocytes. *Autophagy* **2**, 39–46 (2006).
35. W. H. Koppenol, P. L. Bounds, C. V. Dang, Otto Warburg's contributions to current concepts of cancer metabolism. *Nat. Rev. Cancer* **11**, 325–337 (2011).
36. Y. Sun *et al.*, miR-142 controls metabolic reprogramming that regulates dendritic cell activation. *J. Clin. Invest.* **129**, 2029–2042 (2019).
37. Q. Chen, E. J. Vazquez, S. Moghaddas, C. L. Hoppel, E. J. Lesnefsky, Production of reactive oxygen species by mitochondria: Central role of complex III. *J. Biol. Chem.* **278**, 36027–36031 (2003).
38. Z. Yin *et al.*, Structural basis for a complex I mutation that blocks pathological ROS production. *Nat. Commun.* **12**, 707 (2021).
39. F. de Nigris *et al.*, Oxidation-sensitive mechanisms, vascular apoptosis and atherosclerosis. *Trends Mol. Med.* **9**, 351–359 (2003).
40. M. P. Mattson, Neuronal life-and-death signaling, apoptosis, and neurodegenerative disorders. *Antioxid. Redox Signal.* **8**, 1997–2006 (2006).
41. S. S. Correia, A. G. McGrath, A. Lee, A. M. Graybiel, K. A. Goosens, Amygdala-ventral striatum circuit activation decreases long-term fear. *eLife* **5**, e12669 (2016).
42. S. Hormigo, G. Vega-Flores, M. A. Castro-Alamancos, Basal ganglia output controls active avoidance behavior. *J. Neurosci.* **36**, 10274–10284 (2016).
43. P. J. Fernandez-Marcos, J. Auwerx, Regulation of PGC-1α, a nodal regulator of mitochondrial biogenesis. *Am. J. Clin. Nutr.* **93**, 884S–890S (2011).
44. R. Cartoni *et al.*, Mitofusins 1/2 and ERRalpha expression are increased in human skeletal muscle after physical exercise. *J. Physiol.* **567**, 349–358 (2005).
45. I. Kang, C. T. Chu, B. A. Kaufman, The mitochondrial transcription factor TFAM in neurodegeneration: Emerging evidence and mechanisms. *FEBS Lett.* **592**, 793–811 (2018).
46. D. P. Kelly, R. C. Scarpulla, Transcriptional regulatory circuits controlling mitochondrial biogenesis and function. *Genes Dev.* **18**, 357–368 (2004).
47. Z. Wu *et al.*, Mechanisms controlling mitochondrial biogenesis and respiration through the thermogenic coactivator PGC-1. *Cell* **98**, 115–124 (1999).
48. O. J. Martin *et al.*, A role for peroxisome proliferator-activated receptor γ coactivator-1 in the control of mitochondrial dynamics during postnatal cardiac growth. *Circ. Res.* **114**, 626–636 (2014).
49. Y. Ge *et al.*, Two forms of Opa1 cooperate to complete fusion of the mitochondrial inner-membrane. *eLife* **9**, e50973 (2020).
50. C. R. Chang, C. Blackstone, Cyclic AMP-dependent protein kinase phosphorylation of Drp1 regulates its GTPase activity and mitochondrial morphology. *J. Biol. Chem.* **282**, 21583–21587 (2007).
51. L. C. Gomes, L. Scorrano, High levels of Fis1, a pro-fission mitochondrial protein, trigger autophagy. *Biochim. Biophys. Acta* **1777**, 860–866 (2008).
52. I. Tanida, T. Ueno, E. Kominami, LC3 and autophagy. *Methods Mol. Biol.* **445**, 77–88 (2008).
53. S. Pickles, P. Vigié, R. J. Youle, Mitophagy and quality control mechanisms in mitochondrial maintenance. *Curr. Biol.* **28**, R170–R185 (2018).
54. D. G. Hardie, Minireview: The AMP-activated protein kinase cascade: The key sensor of cellular energy status. *Endocrinology* **144**, 5179–5183 (2003).
55. M. Yamamoto *et al.*, Regulation of oxidative stress by the anti-aging hormone klotho. *J. Biol. Chem.* **280**, 38029–38034 (2005).
56. W. Xiao, R. S. Wang, D. E. Handy, J. Loscalzo, NAD(H) and NADP(H) redox couples and cellular energy metabolism. *Antioxid. Redox Signal.* **28**, 251–272 (2018).
57. X. Cao, L. Wu, J. Zhang, M. Dolg, Density functional studies of coenzyme NADPH and its oxidized form $NADP^+$: Structures, UV-Vis spectra, and the oxidation mechanism of NADPH. *J. Comput. Chem.* **41**, 305–316 (2020).
58. Q. Chen *et al.*, The late increase in intracellular free radical oxygen species during apoptosis is associated with cytochrome c release, caspase activation, and mitochondrial dysfunction. *Cell Death Differ.* **10**, 323–334 (2003).
59. D. H. Geschwind, P. Levitt, Autism spectrum disorders: Developmental disconnection syndromes. *Curr. Opin. Neurobiol.* **17**, 103–111 (2007).
60. A. Anitha *et al.*, Brain region-specific altered expression and association of mitochondria-related genes in autism. *Mol. Autism* **3**, 12 (2012).
61. R. E. Frye *et al.*, Mitochondrial dysfunction may explain symptom variation in Phelan–McDermid syndrome. *Sci. Rep.* **6**, 19544 (2016).
62. A. M. Lepagnol-Bestel *et al.*, SLC25A12 expression is associated with neurite outgrowth and is upregulated in the prefrontal cortex of autistic subjects. *Mol. Psychiatry* **13**, 385–397 (2008).
63. N. Cheng, J. M. Rho, S. A. Masino, Metabolic dysfunction underlying autism spectrum disorder and potential treatment approaches. *Front. Mol. Neurosci.* **10**, 34 (2017).
64. A. K. Kanellopoulos *et al.*, Aralar sequesters GABA into hyperactive mitochondria, causing social behavior deficits. *Cell* **180**, 1178–1197.e20 (2020).
65. V. Costa, L. Scorrano, Shaping the role of mitochondria in the pathogenesis of Huntington's disease. *EMBO J.* **31**, 1853–1864 (2012).
66. R. J. Ferrante, N. W. Kowall, E. P. Richardson Jr,, Proliferative and degenerative changes in striatal spiny neurons in Huntington's disease: A combined study using the section-Golgi method and calbindin D28k immunocytochemistry. *J. Neurosci.* **11**, 3877–3887 (1991).
67. A. S. C. Louis Sam Titus *et al.*, Reduced expression of Foxp1 as a contributing factor in Huntington's disease. *J. Neurosci.* **37**, 6575–6587 (2017).
68. B. Tang *et al.*, Forkhead box protein p1 is a transcriptional repressor of immune signaling in the CNS: Implications for transcriptional dysregulation in Huntington disease. *Hum. Mol. Genet.* **21**, 3097–3111 (2012).
69. J. K. McGill, M. F. Beal, PGC-1α, a new therapeutic target in Huntington's disease? *Cell* **127**, 465–468 (2006).
70. L. Cui *et al.*, Transcriptional repression of PGC-1alpha by mutant huntingtin leads to mitochondrial dysfunction and neurodegeneration. *Cell* **127**, 59–69 (2006).
71. P. Jonas, C. Racca, B. Sakmann, P. H. Seeburg, H. Monyer, Differences in Ca^{2+} permeability of AMPA-type glutamate receptor channels in neocortical neurons caused by differential GluR-B subunit expression. *Neuron* **12**, 1281–1289 (1994).
72. S. Melzer *et al.*, Distinct corticostriatal GABAergic neurons modulate striatal output neurons and motor activity. *Cell Rep.* **19**, 1045–1055 (2017).
73. A. G. Carter, B. L. Sabatini, State-dependent calcium signaling in dendritic spines of striatal medium spiny neurons. *Neuron* **44**, 483–493 (2004).
74. D. L. Rousso, Z. B. Gaber, D. Wellik, E. E. Morrisey, B. G. Novitch, Coordinated actions of the forkhead protein Foxp1 and Hox proteins in the columnar organization of spinal motor neurons. *Neuron* **59**, 226–240 (2008).
75. D. J. Socci, K. B. Bjugstad, H. C. Jones, J. V. Pattisapu, G. W. Arendash, Evidence that oxidative stress is associated with the pathophysiology of inherited hydrocephalus in the H-Tx rat model. *Exp. Neurol.* **155**, 109–117 (1999).
76. N. Chenouard, J. Buisson, I. Bloch, P. Bastin, J.-C. Olivo-Marin, "Curvelet analysis of kymograph for tracking bi-directional particles in fluorescence microscopy images" in *2010 IEEE International Conference on Image Processing* (2010), pp. 3657–3660.
77. F. de Chaumont *et al.*, Icy: An open bioimage informatics platform for extended reproducible research. *Nat. Methods* **9**, 690–696 (2012).
78. S. Berg *et al.*, ilastik: Interactive machine learning for (bio)image analysis. *Nat. Methods* **16**, 1226–1232 (2019).